Output Mode Switching for Parallel Five-bar Manipulators Using a Graph-based Path Planner

Parker B. Edwards[1], Aravind Baskar[2], Caroline Hills[1], Mark Plecnik[2]*, and Jonathan D. Hauenstein[1]

Abstract— **The configuration spaces of parallel manipulators exhibit more nonlinearity than serial manipulators. Qualitatively, they can be seen to possess extra folds. Projection onto smaller spaces of engineering relevance, such as an output workspace or an input actuator space, these folds cast edges that exhibit boundary behavior. For example, inside the global workspace bounds of a five-bar linkage appear several local workspace bounds that only constrain certain output modes of the mechanism. The presence of such boundaries, which manifest in both input and output projections, serve as a source of confusion when these projections are studied exclusively instead of the configuration space itself. Particularly, the design of nonsymmetric parallel manipulators has been confounded by the presence of exotic projections in their input and output spaces. In this paper, we represent the configuration space with a radius graph, then weight each edge by solving an optimization problem using homotopy continuation to quantify transmission quality. We then employ a graph path planner to approximate geodesics between configuration points that avoid regions of low transmission quality. Our methodology automatically generates paths capable of transitioning between non-neighboring output modes, a motion which involves osculating multiple workspace boundaries (local, global, or both). We apply our technique to two nonsymmetric five-bar examples that demonstrate how transmission properties and other characteristics of the workspace can be selected by switching output modes.**

I. INTRODUCTION

The workspaces of parallel mechanisms are more complicated than their serial counterparts. Their interiors generically contain inner bounds of different sorts: either favorable or unfavorable transmission characteristics, or locations where it is possible to transition between different modes of the mechanism. Dealing with such complexity is a burden, but provides opportunity for kinematical advantages. For example, at a single output point, parallel mechanisms can assume a larger selection of configurations that afford more choice of directional transmission characteristics.

More precisely, consider the case where a mechanism's configuration space is implicitly defined as the set of mechanism parameters which satisfy a set of nonlinear constraints. Various subsets of "singular" configurations which exhibit atypical kinematic characteristics may subsequently be defined as satisfying additional equations. The main challenge

reduces to computing paths for transitioning between different modes which avoid problematic configurations, and more generally between any two mechanism configurations. The path planning problem, even polynomial constraints, has time complexity that grows exponentially in the number of parameters (e.g., [1], [2]). Despite this, considerable interest in the problem has correspondingly resulted in a number of proposed methods for singularity-free path planning and analyzing configuration spaces with singularities removed in practical situations, see [3], [4], [5], [6], [7], [8] for a non-exhaustive list. The automatic methods in this list approximate the singularity-free configuration space of a mechanism in various ways, and share a requirement for a user-supplied input sometimes called a *resolution*. The resolution controls how closely the configuration space's geometry is approximated during path planning. Typical theoretical guarantees show that a method is resolution-complete: "[...] it always returns a path if one exists at a given resolution, or returns 'failure' otherwise" [3].

We present here a proof of concept path planning method which integrates recently developed numerical algebraic geometry [9], [10] approaches to compute geometric feature sizes [11], [12], dense samples [13], [14], and Euclidean distance to singular sets [15]. This yields a deterministic path planner with stronger guarantees than resolution-completeness. For a given input space, there is a correct resolution at which our path planner returns a path if one exists, reports that no path exists otherwise, and the method automatically estimates this resolution in a principled way.

The resulting output is a weighted graph whose nodes are points in the configuration space and edges are weighted by distance in the ambient space. Building a global graph-based model in this fashion is currently more computationally expensive than other proposals. Our approach's most novel elements however, namely feature size and Euclidean distance-to-singularity computations, are fast and can be integrated with other proposals. The graph models we compute are effective, allowing us to compute shortest paths that closely estimate configuration space geodesics and make repeated queries to investigate the geometry of different modes.

II. BACKGROUND

Let us compare the serial 2R mechanism (Fig. 1, left) to a parallel five-bar (Fig. 1, right). The workspace of the 2R is an annulus. It can assume two different configurations for every point within its x-y workspace. To transition between these points, the end-effector point must travel to a workspace bound and come back. Placing a rotary actuator at each joint,

[1]Parker B. Edwards, Caroline Hills, and Jonathan D. Hauenstein are with Department of Applied and Computational Mathematics and Statistics, University of Notre Dame, Notre Dame, IN 46556 USA {`parker.edwards,chills1,hauenstein`}@nd.edu

[2]Aravind Baskar and Mark Plecnik are with Department of Aerospace and Mechanical Engineering, University of Notre Dame, Notre Dame, IN 46556 USA {`abaskar,plecnikmark`}@nd.edu
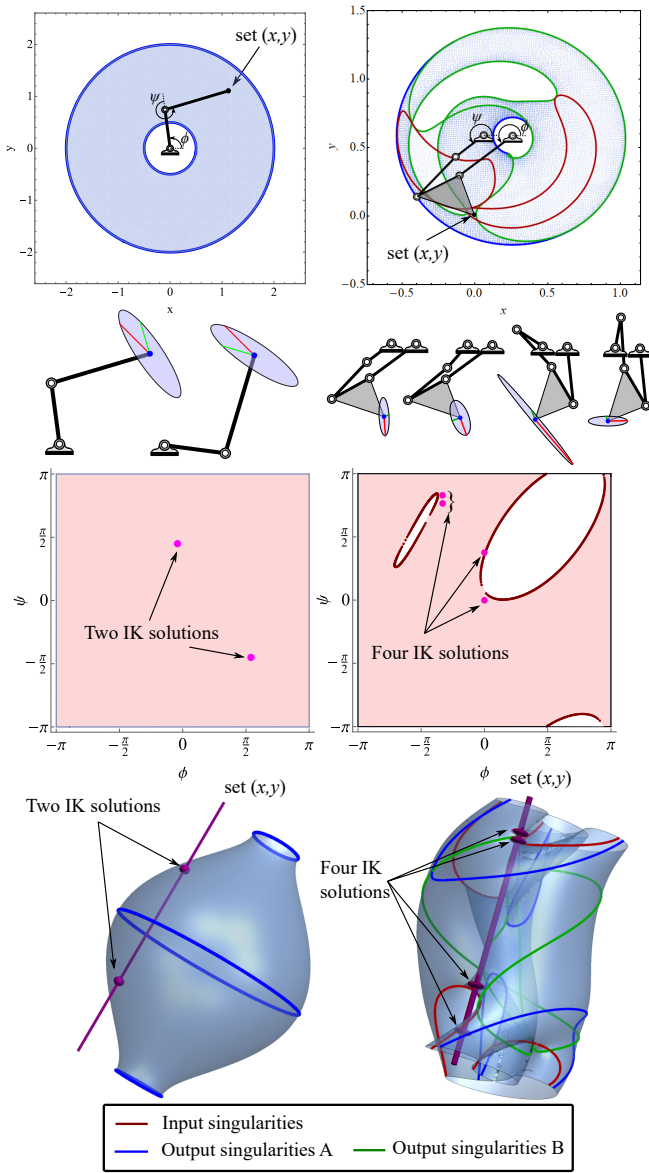
Fig. 1. Views of the configuration spaces of a serial 2R (left) and a parallel five-bar (right). 1st row: The output workspace for each manipulator. 2nd row: The 2R admits two IK solutions, the five-bar admits four. 3rd row: The input actuator space for each manipulator, with holes visible for the five-bar. 4th row: An (x, y, ψ) view of the configuration manifold. The skewering line shows the locations of the IK solutions for a set (x, y).

there are no points in the workspace where the linkage is incapable of exerting a force in any direction. At each point, the selection of configurations and velocity ellipses [16] available are reflections of one another, see Fig. 1.

The workspace bounds of a five-bar is a union of two circular arc segments and two four-bar coupler curves. Despite having two degrees-of-freedom, its configuration space cannot be fully visualized with only two parameters. Therefore, viewing the x-y projection of its configuration space seemingly shows additional interior workspace bounds. To add to the confusion, each internal curve of Fig. 1 is relevant only to certain output modes and irrelevant to others. Some of these bounds indicate holes analogous to the annulus while others indicate bounds of specific output modes which

serve as places of transition between modes. Scattered within its configuration space are curves at which this linkage loses its ability to exert forces in a direction. These curves as well are only relevant to some output modes but not others. For a regular workspace point, the linkage can assume two or four different configurations, with each exhibiting a different velocity ellipse. To study these configuration spaces, we use the terms *input singularities*, *output singularities*, *input modes*, and *output modes*.

Input singularities. Input singularities are the singular solutions to the forward kinematics problem. They serve as *local* bounds of motion in the input space, e.g. the ϕ-ψ plane (Fig. 1). At these bounds, one of the semi-axis lengths of the velocity ellipse in output space tends toward infinity. It is in that direction that the linkage cannot transmit any force at the end-effector no matter the torque exerted by the actuators. Because of this loss of control authority, input singularities are generally considered to have **transmission problems** and should be avoided. For a five-bar linkage, the geometric condition for an input singularity is that points C, D, F, are collinear (Fig. 2). The literature also uses the terminology *type II singularity* [17] and *DKP* (direct kinematic problem) *singularity* [18]. *Input singularity* is used in [4], or *forward singularity* to include cases induced by a nonsmooth configuration space.

Output singularities. Output singularities are the singular solutions to the inverse kinematics problem. They serve as *local* bounds of motion in the output space, e.g. the x-y plane (Fig. 1). At these bounds, the semi-axis of the velocity ellipse normal to these curves collapses to zero. It is in that direction that the linkage can sustain any force at the end-effector with zero torque from the actuators. In this way, there are **no transmission problems** at output singularities from the vantage of torque exerted by the actuators. It is at these configurations that the linkage is able to transition output modes. For a five-bar linkage, the geometric condition for an output singularity is that either points A, C, P, or points B, D, F, are collinear (Fig. 2). The literature also uses the terminology *type I singularity* [17] and *IKP* (inverse kinematic problem) *singularity* [18]. *Output singularity* is used in [4], or *inverse singularity* to include cases induced by a nonsmooth configuration space.

Input modes. The separated regions that result after partitioning the configuration space by its input singularities are called its input modes. Note that if input singularities do not exist, there may still be more than one input mode, depending on the connectivity of the unpartitioned configuration space. An input mode is a maximal continuous region of configurations whereby a path can be formed between any two regular interior members without passing through an input singularity. The term *assembly mode* appears frequently in past literature. An *input mode* is not an *assembly mode*. As defined in the past, the total number of assembly modes is equal to the number of solutions to the forward kinematics problem, implying the solutions uniquely identify all assembly modes. The total number of input modes could be less than, equal, or greater than the number of assembly modes.
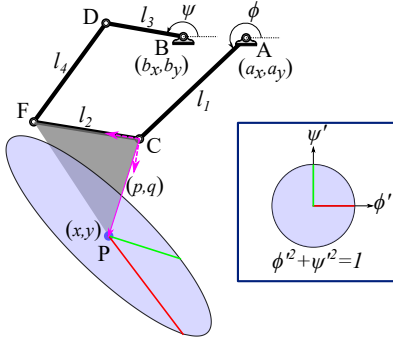
Fig. 2. Schematic of a five-bar mechanism. The velocity ellipse with respect to the input angles ϕ and ψ is shown at its end-effector (x, y).

One way that it may be less is when a path exists between two forward kinematics solutions that does not pass through an input singularity, hence they are part of the same input mode. Such cases are well documented and illustrate the shortcomings of the term *assembly mode* [19]. The number of input modes is greater than the number of assembly modes when the unpartitioned configuration space already consists of disconnected regions which are further divided by the presence of input singularities.

Output modes. Similarly to input modes, the separated regions that result after partitioning the configuration space by its output singularities are called its output modes. Note that if output singularities do not exist, there may still be more than one output modes, depending on the connectivity of the unpartitioned configuration space. An output mode is a maximal continuous region of configurations whereby a path can be formed between any two regular interior members without passing through an output singularity. The term *working mode* appears frequently in past literature. An *output mode* is not a *working mode*. As defined in the past, the total number of working modes is equal to the number of solutions to the inverse kinematics problem, implying the solutions uniquely identify all working modes. The total number of output modes could be less than, equal, or greater than the number of working modes. One way that it may be less is when a path exists between two inverse kinematics solutions that does not pass through an output singularity, hence they are part of the same output mode. The number of output modes is greater than the number of working modes when the unpartitioned configuration space already consists of disconnected regions which are further divided by the presence of output singularities.

III. METHOD

Let $C \subset \mathbb{R}^n$ denote the d-dimensional configuration space which is a manifold[1] in the n-dimensional ambient space such that C is defined by the system of $n - d$ polynomial equations $\mathbf{F}(\mathbf{z}) = 0$ where $\mathbf{z} \in \mathbb{R}^n$. Suppose that the set of input singularities I in the configuration space is defined by the polynomial equation $g(\mathbf{z}) = 0$ where $\mathbf{z} \in C$. For instance, consider the five-bar mechanism as depicted in Fig. 2.

---

[1]Recall that manifolds do not have self-intersections, cusps, or other geometric singularities.

The dimensions are given by $a_x, a_y, b_x, b_y, l_1, l_2, l_3, l_4, p, q$. For canonical representation, $a_x = a_y = b_y = 0$ can be assumed without loss of generality. The configuration space is defined by $\mathbf{F}(\mathbf{z}) = 0$:

$$x^2 + y^2 - 2l_1\left(xc_\phi + ys_\phi\right) + l_1^2 - p^2 - q^2 = 0,$$

$$l_2^2(x^2 + y^2) + l_1^2((l_2 - p)^2 + q^2) + (b_x^2 + l_3^2 - l_4^2)(p^2 + q^2)$$
$$-2l_2l_3(p(xc_\psi + ys_\psi) - q(xs_\psi - yc_\psi)) - 2b_xl_2(px + qy)$$
$$+2l_1l_3((l_2p - p^2 - q^2)(c_\phi c_\psi + s_\phi s_\psi) + 2b_xl_3(p^2 + q^2)c_\psi$$
$$+2b_xl_1((l_2p - p^2 - q^2)c_\phi + l_2qs_\phi) - 2l_1l_2l_3q(c_\phi s_\psi - s_\phi c_\psi)$$
$$+2l_1l_2((p - l_2)(xc_\phi + ys_\phi) - q(xs_\phi - yc_\phi)) = 0,$$

$$c_\phi^2 + s_\phi^2 - 1 = 0, \qquad c_\psi^2 + s_\psi^2 - 1 = 0,$$

where the variables are $\mathbf{z} = (x, y, c_\phi, s_\phi, c_\psi, s_\psi)$ with c_ϕ, s_ϕ and c_ψ, s_ψ being the cosine and the sine of ϕ and ψ in order, respectively. Consider our work to take a characteristic length [20] of unity. The replacement of angles with their corresponding cosine and sine along with the Pythagorean identity is a standard approach to yield polynomials and it avoids redundancy related to the periodicity of angles. In particular, other than an increased number of variables and equations, this does not impact the results of path planning.

Let $\mathbf{F}_1$ and $\mathbf{F}_2$ be the first two polynomial functions above. For the five-bar, the set of input singularities I is defined by

$$g(\mathbf{z}) = \det \begin{pmatrix} \frac{\partial \mathbf{F}_1}{\partial x} & \frac{\partial \mathbf{F}_1}{\partial y} \\ \frac{\partial \mathbf{F}_2}{\partial x} & \frac{\partial \mathbf{F}_2}{\partial y} \end{pmatrix} = 0 \quad \text{for } \mathbf{z} \in C.$$

A first measure of the geometric complexity of I is its degree in the ambient space. Generically, for the five-bar, I is a union of two irreducible curves of degree 6. Note that these two curves arise from two four-bar coupler curves.

A. Sampling and graph construction

The graph construction will follow a straightforward radius graph approach. For $\mathbf{v} \in \mathbb{R}^n$, let $\|\mathbf{v}\|$ denote the standard Euclidean distance. For $r > 0$, the r-radius graph on a finite set $\hat{C} \subset \mathbb{R}^n$, denoted $G_r(\hat{C})$, is the undirected graph with node set $\hat{C}$ and an edge $\mathbf{e} = (\mathbf{c_0}, \mathbf{c_1})$ that is weighted by distance $\|\mathbf{c_0} - \mathbf{c_1}\|$ for every pair of distinct points $\mathbf{c_0}, \mathbf{c_1} \in \hat{C}$ such that $\|\mathbf{c_0} - \mathbf{c_1}\| \leq r$.

To model the configuration space C with a radius graph, we require an appropriate finite sample[2] $\hat{C} \subset C$ and also an appropriate radius $r > 0$. To be more precise regarding the sample, our method first determines an appropriate "resolution" $\epsilon > 0$ and then computes an ϵ-*sample* of C, $\hat{C}$, such that every point $\mathbf{c} \in C$ is within distance ϵ of a point in $\hat{C}$.

We can associate to C two geometric feature sizes: the *reach* of C [21], denoted $\mathrm{reach}(C)$, and the *weak feature size* of C [22], [23], denoted $\mathrm{wfs}(C)$. These are numbers which, roughly speaking, quantify the size of the geometric features in C. They are related by $0 < \mathrm{reach}(C) \leq \mathrm{wfs}(C)$. See, e.g., [12, Sec. 2] for an expanded discussion. One can show (e.g., [12, Thm 2.11]) that if $2\epsilon < \mathrm{wfs}(C)$, $\hat{C}$ is an ϵ-sample

---

[2]In fact, we can easily relax the requirement $\hat{C} \subset C$ to allow the set $\hat{C}$ to consist of points which are at most distance $\delta > 0$ from C for small δ. For the sake of clarity, we discuss the case where $\delta = 0$.

of C. Moreover, if $r(\epsilon) = 4\epsilon$, then any path of edges in the radius graph $G_{r(\epsilon)}(\hat{C})$ maps continuously onto a path in C and $G_{r(\epsilon)}(\hat{C})$ has the same number of connected components as C. Additionally, if $2\epsilon < \text{reach}(C)$, then for any edge $(\mathbf{c_0}, \mathbf{c_1}) \in G_{r(\epsilon)}(\hat{C})$, there is a path in C between $\mathbf{c_0}$ and $\mathbf{c_1}$ where the distance $\|\mathbf{c_0} - \mathbf{c_1}\|$ is a good estimate for the length of the path. The shortest path graph distance between two points in $G_{r(\epsilon)}(\hat{C})$ is subsequently a good estimate for the shortest path distance in C between the points.

Numerical algebraic geometry methods which use the polynomial system $\mathbf{F}$ to determine the reach and weak feature size of C have recently been developed [11], [12], as have methods which produce an ϵ-sample of C from $\mathbf{F}$ [13], [14]. One advantage of the latter method over, e.g., random sampling, is that we can use geometric subsampling methods to mitigate oversampling while maintaining an appropriate resolution. Verifiably computing feature sizes remains relatively expensive, but there are principled early stopping criteria to estimate[3] $\text{wfs}(C)$ inexpensively. In summary, we construct a graph to model C as follows:

1) Compute an estimate W for $\text{wfs}(C)$ using the polynomial system $\mathbf{F}$ as input.
2) Compute an ϵ-sample of C, $\hat{C}$, where $W = 2\epsilon$, using the polynomial system $\mathbf{F}$ as input.
3) Construct the radius graph $G_{r(\epsilon)}(\hat{C})$.

B. Singularity avoidance

An edge in this constructed graph corresponds with a path between two points in the configuration space. To avoid input singularities, one only needs, in theory, to remove edges which correspond to paths that cross the input boundary. Since we cannot check this directly, we instead compute the distance in the ambient space between the set of input singularities and the straight-line segment connecting an edge's two endpoints. This is justified by the heuristic that the straight-line segment between the two points can be taken as a reasonable approximation of the geodesic in the configuration space connecting the two points.

As a brief remark, alternative methods typically use the function $g : \mathbb{R}^n \to \mathbb{R}$, the determinant defining I, for singularity avoidance directly rather than the distance-to-singularity function. A distinct advantage of using Euclidean distance is that it is, in mathematical terms, 1-Lipschitz continuous. Denoting the function by $d_I : \mathbb{R}^n \to \mathbb{R}$, we have $|d_I(\mathbf{z}_1) - d_I(\mathbf{z}_2)| \le \|\mathbf{z}_1 - \mathbf{z}_2\|$ for any $\mathbf{z}_1, \mathbf{z}_2 \in \mathbb{R}^n$. The function g is continuous, but in contrast can easily send nearby inputs to very different values.

Let $\mathbf{c}_0, \mathbf{c}_1 \in C$ so that the straight-line segment connecting them is $\mathbf{c}(t) = (1-t)\mathbf{c}_0 + t\mathbf{c}_1$ for $t \in [0, 1]$. Hence, $\mathbf{c}(0) = \mathbf{c}_0$ and $\mathbf{c}(1) = \mathbf{c}_1$. We aim to solve

$$\min\{\|\mathbf{c}(t) - \mathbf{w}\|^2 \ : \ \mathbf{w} \in I, 0 \le t \le 1\}. \quad (1)$$

Utilizing the Fritz John first-order necessary conditions, one

[3]Following the terminology of [12], we compute only the geometric 2-bottlenecks of C.

obtains the polynomial system $\mathbf{J}(\mathbf{w}, t, \lambda)$ equal to

$$\begin{bmatrix} \mathbf{F}(\mathbf{w}) \\ g(\mathbf{w}) \\ \lambda_0 \nabla_{\mathbf{w},t} \left(\|\mathbf{c}(t) - \mathbf{w}\|^2 \right) + \sum_{i=1}^d \lambda_i \nabla_{\mathbf{w},t} \left(\mathbf{F}_i(\mathbf{w}) \right) \\ + \lambda_{d+1} \nabla_{\mathbf{w},t} \left(g(\mathbf{w}) \right) + \lambda_{d+2} \nabla_{\mathbf{w},t} \left(t \right) + \lambda_{d+3} \nabla_{\mathbf{w},t} \left(1 - t \right) \\ \lambda_{d+2} t \\ \lambda_{d+3}(1 - t) \end{bmatrix}$$

where $\lambda \in \mathbb{P}^{d+3}$ and $\nabla_{\mathbf{w},t}(f(\mathbf{w}, t))$ is the gradient vector of $f(\mathbf{w}, t)$ with respect to $\mathbf{w}$ and t for any function f.

Since we aim to solve $\mathbf{J} = 0$ for various choices of $\mathbf{c}_0$ and $\mathbf{c}_1$, we employ a parameter homotopy [24] with $\mathbf{c}_0$ and $\mathbf{c}_1$ as parameters. Thus, the first step is perform an *ab initio* solve of $\mathbf{J} = 0$ for generic values of the parameters. Note that the system $\mathbf{J}$ has a natural two-homogeneous structure with variables groups $(\mathbf{w}, t)$ and λ. Hence, a multihomogeneous homotopy or a multihomogeneous regeneration [25], [26] can be employed for this *ab initio* solve. Then, a parameter homotopy simply deforms from the generic values of the parameter to the given values of $\mathbf{c}_0$ and $\mathbf{c}_1$. The number of solution paths tracked in this parameter homotopy is precisely the generic number of solutions to $\mathbf{J} = 0$. For the five-bar, the two-homogeneous Bézout count of $\mathbf{J}$ is 1152 while the actual generic number of solutions to $\mathbf{J} = 0$ is 84.

The endpoints of the parameter homotopy correspond with critical points of (1) for the given values of $\mathbf{c}_0$ and $\mathbf{c}_1$. Hence, one can solve (1) by sorting through the critical points to determine real critical points on the line segment, i.e., for $t \in [0, 1]$, and selecting the corresponding minimum distance. Moreover, by considering the last two polynomials in $\mathbf{J}$, which correspond to the complimentary slackness condition, one can actually break the computation into three separate pieces: at $t = 0$, at $t = 1$, and along the interior of the line segment, i.e., for $0 < t < 1$. Corresponding parameter homotopies would track 24, 24, and 36 paths, respectively, with $24 + 24 + 36 = 84$. Since many edges in the graph can have the same node, one advantage of breaking this computation into these three separate pieces is to avoid recomputing the same information for repeated nodes.

Performing this computation for every edge $\mathbf{e}$ in the constructed graph results in a minimum distance $D(\mathbf{e})$ along that edge to the input singularity and a distance $D(\mathbf{c})$ for every configuration $\mathbf{c}$ in the node set $\hat{C}$. To use the graph for singularity avoidance, i.e., to model the space $C \setminus I$, we then choose a distance threshold T and remove all edges from the graph with $D(\mathbf{e}) < T$. Any remaining nodes with no edges are also removed. In principle, one would like to compute a threshold T such that the reduced graph has as many connected components as input modes. This would require a distinct and currently infeasible feature size computation for I as a subspace of the manifold C. At the present, we instead choose $T = r(\epsilon)$ based on simple geometric heuristics. Note, however, that we can also choose T based on engineering considerations. Singularity-avoiding path planning queries can be subsequently performed by shortest path computations in this graph, e.g., with A^* path planning [27] using the Euclidean distance in ambient space between two configurations as a heuristic.

C. Computational considerations

A full computational complexity analysis is beyond the scope of this work, but we include here some heuristics for consideration as well as order-of-magnitude timing information from an implemented version of the method applied to the two examples in Section IV. Most computations were performed on a 24 CPU Intel Xeon E5-2680 at 2.50GHz.

Estimating wfs(C). This is a homotopy continuation computation with costs one expects to increase based on the number of variables n, codimension $n - d$ of C, and degree of the polynomials in F increase. In Section IV, $n = 6$ with codimension 4 and degree of the polynomials is 2. Estimating wfs(C) for Example 2 in Section IV with 24 cores required approximately 6 minutes. These computations are easily parallelizable and so can readily utilize additional CPUs.

Computing an ϵ-sample. This procedure relies upon homotopy continuation methods that also scale in the number of variables, codimension of C, and degree of the polynomials in F. Costs also increase with the number of sample points. Heuristically, one expects the number of sample points to scale with $\left(\frac{\text{vol}_d(C)}{W}\right)^d$ where $\text{vol}_d(C)$ is the d-dimensional Hausdorff measure of C. For additional experimental results regarding the number of points, see [13]. With 24 CPU cores, the examples in Section IV required approximately a day of computation. Subsequently, computing a radius graph from the sample required on the order of minutes.

Computing the input boundary distance $D(\mathbf{e})$. For a single edge $\mathbf{e}$, computing $D(\mathbf{e})$ is a homotopy continuation computation with similar considerations to those previously discussed. For example, using a single core, a typical edge computation for Example 2 in Section IV required 0.8 seconds. The implementation used for this manuscript computes $D(\mathbf{e})$ for every edge $\mathbf{e}$ in the computed radius graph, which scales with the number of points in the sample. Computations for each edge can easily be done in parallel. Moreover, the same example required approximately 11.75 hours to compute $D(\mathbf{e})$ for 3.2×10^6 edges using 6 servers, each with either 24 or 32 CPUs. Note that, after an initial step computing minimum distances from the graph nodes to the singularity set, one may use that information to forego computing $D(\mathbf{e})$ for any edge $\mathbf{e}$ with endpoints sufficiently far away from I relative to the singularity avoidance threshold T.

Example	a_x	b_x	p	l_1	l_2
1	0.259	0.060	0.049	0.465	0.349
2	0.066	−0.642	0.298	0.775	0.832

Example	a_y	b_y	q	l_3	l_4
1	0.586	0.590	0.328	0.249	0.411
2	0.815	0.845	1.304	0.291	0.522

TABLE I

FIVE-BAR DIMENSIONS FOR THE TWO EXAMPLES

Example	# pts in graph	# edges in graph
1	82,581	2.3×10^6
2	121,667	3.2×10^6

TABLE II

SUMMARY OF THE RADIUS GRAPHS FOR THE TWO EXAMPLES

IV. RESULTS

The methodologies described above were applied to two examples of nonsymmetric five-bar linkages. Their parameters are listed in Table I with Table II summarizing the size of the graphs computed. Both examples involve traversing across non-neighboring output modes while maintaining the same input mode. In other words, output singularities are crossed and input singularities are not.

Example 1: Perpendicular velocity ellipses at an x-y point

The first example five-bar possesses a point in its workspace where two of the four IKP solutions exhibit velocity ellipses with a 4:1 aspect ratio that are perpendicular to each other. Its dimensions were found using the method reported in [28]. The direction of the short axis benefits from 4x larger force transmission while the direction of the long axis can achieve 4x greater speeds. The configurations corresponding to these perpendicular velocity ellipses are housed in different output modes. The path planning challenge is to approximate the geodesic from one to the other, which in this case involves transitioning through at least two output singularities. A feasible path designed using our methodology for this challenge is shown in Fig. 4.

At the computed singularity avoidance threshold, the graph model of the configuration space estimated 6 input modes, 5 output modes, and 7 input/output modes (maximal regions bounded by both input and output singularities). Due to the numerical threshold, our counts generally do not match the true number of regions, as they partition the configuration space with a thicker kerf, so to say. In some respects, this is more practical as input singularities should be avoided by a margin of safety. To give some idea of the space's extrinsic curvature, the distance in ambient space between the two configurations of interest is 2.11, the shortest path in the configuration space estimated by our method without input singularity avoidance is 2.66, and the shortest point with input singularity avoidance is 2.74.

Example 2: A ceiling and a floor

The second example five-bar possesses an output mode where there exists an arc that serves as a local upper bound for the y-coordinate of the end-effector, referred to as a *ceiling*. The same five-bar also possesses another output mode where there exists another arc, nearly on top of the first arc, but now functioning as a local lower bound for the y-coordinate of the end-effector, referred to as a *floor*. The path planning challenge is to transition from the output mode with a ceiling to the output mode with a floor. This could be useful because, at an output bound, the mechanism is able to support large loads in the bound's normal direction without any actuator effort. However, as it is a bound, regular motions can only take place on one side, locally. By transitioning between a ceiling and a floor, the side of regular motion becomes selectable. Fig. 6 shows a feasible path designed using the methodology presented for this example.

Our method estimated 5 input modes, 3 output modes, and 12 input/output modes. The ambient distance between
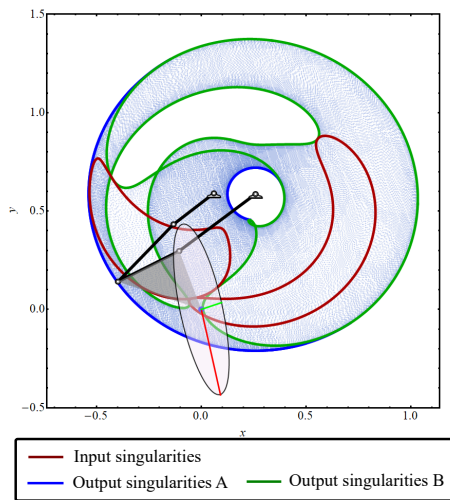
Fig. 3. Example 1: At the x-y point shown, there exists another configuration with a velocity ellipse perpendicular to the one displayed.
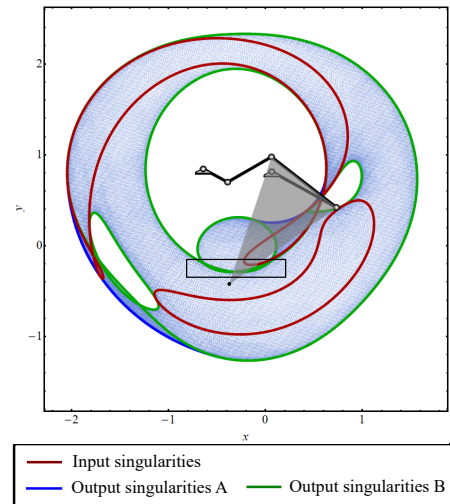

Fig. 5. Example 2: The portion of the output bound which functions as a ceiling or floor is indicated with a box.
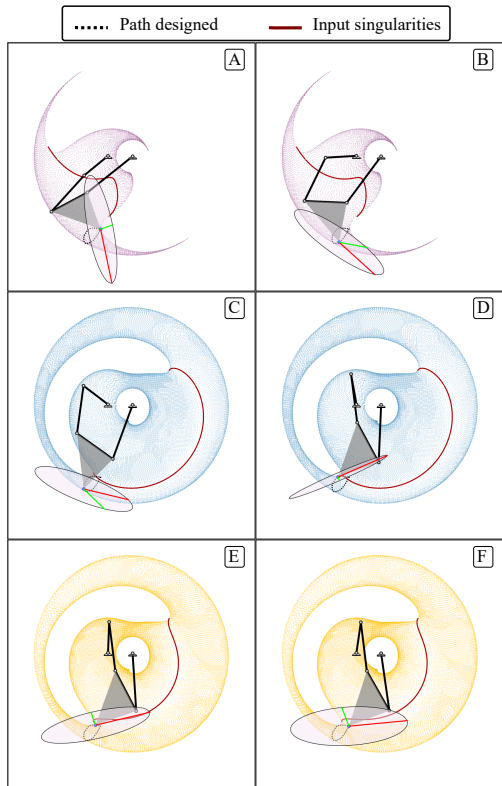

Fig. 4. Example 1: A feasible path marked with six snapshots, marked alphabetically from A to E, to switch between the configurations corresponding to two perpendicular velocity ellipses. The workspace and the input singularity curves shown correspond to the output mode to which each configuration belongs. Output modes are distinguished by color.
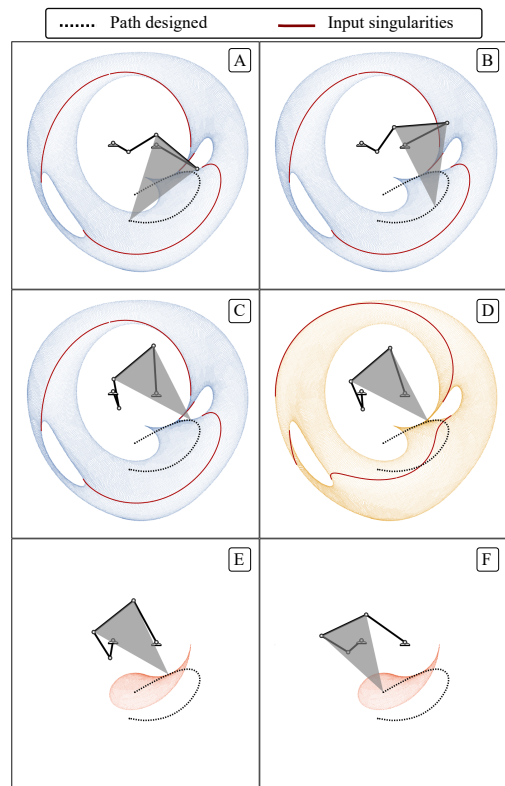

Fig. 6. Example 2: A feasible path marked with six snapshots, marked alphabetically from A to E, for the ceiling-to-floor example. The workspace and the input singularity curves shown correspond to the output mode to which each configuration belongs. Output modes are distinguished by color.

the configuration in Fig. 6 was 2.61 and the path distance both with and without input singularity avoidance was 4.82. The two paths distances are the same since the computed path does not come particularly close to an input singularity.

V. CONCLUSIONS

This paper presented a motion planning technique for transitioning between points in the configuration space of a five-bar manipulator. This is a challenging task since the input and output singularities of parallel manipulators appear in a complicated manner. To overcome this, we constructed a radius graph to represent the workspace with edges weighted by nearness to input singularities. The graph is partitioned into input modes and a path planner is employed to approximate geodesics between start and final points that avoid input singularities. The resulting algorithm is able to traverse through multiple output modes in a smooth manner as demonstrated with two examples.

REFERENCES

[1] J. Canny, *The complexity of robot motion planning*. MIT press, 1988.

[2] S. Basu, M.-F. Roy, M. Safey El Din, and E. Schost, "A baby step–giant step roadmap algorithm for general algebraic sets," *Found. Comput. Math.*, vol. 14, no. 6, pp. 1117–1172, 2014. [Online]. Available: https://doi-org.proxy.library.nd.edu/10.1007/s10208-014-9212-1

[3] O. Bohigas, M. E. Henderson, L. Ros, and J. M. Porta, "A singularity-free path planner for closed-chain manipulators," in *2012 IEEE International Conference on Robotics and Automation*. IEEE, 2012, pp. 2128–2134.

[4] O. Bohigas, M. Manubens, and L. Ros, *Singularities of Robot Mechanisms: Numerical Computation and Avoidance Path planning*. Springer, 2016, vol. 41.

[5] S. Caro, D. Chablat, A. Goldsztejn, D. Ishii, and C. Jermann, "A branch and prune algorithm for the computation of generalized aspects of parallel robots," *Artificial Intelligence*, vol. 211, pp. 34–50, 2014. [Online]. Available: https://www.sciencedirect.com/science/article/pii/S0004370214000125

[6] M. E. Henderson, "Multiple parameter continuation: computing implicitly defined k-manifolds," *Internat. J. Bifur. Chaos Appl. Sci. Engrg.*, vol. 12, no. 3, pp. 451–476, 2002. [Online]. Available: https://doi.org/10.1142/S0218127402004498

[7] E. Macho, O. Altuzarra, C. Pinto, and A. Hernandez, "Workspaces associated to assembly modes of the 5R planar parallel manipulator," *Robotica*, vol. 26, no. 3, pp. 395–403, May 2008.

[8] A. Müller and D. Zlatanov, *Singular Configurations of Mechanisms and Manipulators*. Springer, 2019.

[9] D. J. Bates, J. D. Hauenstein, A. J. Sommese, and C. W. Wampler, *Numerically solving polynomial systems with Bertini*, ser. Software, Environments, and Tools. Society for Industrial and Applied Mathematics (SIAM), Philadelphia, PA, 2013, vol. 25.

[10] A. J. Sommese and C. W. Wampler, II, *The numerical solution of systems of polynomials arising in engineering and science*. World Scientific Publishing Co. Pte. Ltd., Hackensack, NJ, 2005.

[11] D. Eklund, "The numerical algebraic geometry of bottlenecks," *Advances in Applied Mathematics*, vol. 142, p. 102416, 2023.

[12] S. Di Rocco, P. B. Edwards, D. Eklund, O. Gäfvert, and J. D. Hauenstein, "Computing geometric feature sizes for algebraic manifolds," *arXiv preprint arXiv:2209.01654*, 2022.

[13] S. Di Rocco, D. Eklund, and O. Gäfvert, "Sampling and homology via bottlenecks," *Mathematics of Computations, to appear*, 2022.

[14] E. Dufresne, P. Edwards, H. Harrington, and J. Hauenstein, "Sampling real algebraic varieties for topological data analysis," in *2019 18th IEEE International Conference On Machine Learning And Applications (ICMLA)*. IEEE, 2019, pp. 1531–1536.

[15] J. D. Hauenstein, "Numerically computing real points on algebraic sets," *Acta Appl. Math.*, vol. 125, pp. 105–119, 2013.

[16] K. M. Lynch and F. C. Park, *Modern Robotics: Mechanics, Planning, and Control*. Cambridge University Press, May 2017.

[17] C. Gosselin and J. Angeles, "Singularity analysis of closed-loop kinematic chains," *IEEE Transactions on Robotics and Automation*, vol. 6, no. 3, pp. 281–290, Jun. 1990.

[18] M. Urizar, V. Petuya, O. Altuzarra, and A. Hernandez, "Computing the Configuration Space for Motion Planning between Assembly Modes," in *Computational Kinematics*, A. Kecskeméthy and A. Müller, Eds. Berlin, Heidelberg: Springer, 2009, pp. 35–42.

[19] A. Hernandez, O. Altuzarra, V. Petuya, and E. Macho, "Defining Conditions for Nonsingular Transitions Between Assembly Modes," *IEEE Transactions on Robotics*, vol. 25, no. 6, pp. 1438–1447, Dec. 2009.

[20] J. Angeles, "Is there a characteristic length of a rigid-body displacement?" *Mechanism and Machine Theory*, vol. 41, no. 8, pp. 884–896, Aug. 2006.

[21] H. Federer, "Curvature measures," *Trans. Amer. Math. Soc.*, vol. 93, pp. 418–491, 1959. [Online]. Available: https://doi-org.proxy.library.nd.edu/10.2307/1993504

[22] F. Chazal and A. Lieutier, "Weak feature size and persistent homology: computing homology of solids in $\mathbb{R}^n$ from noisy data samples," in *Proceedings of the twenty-first annual symposium on Computational geometry*. ACM, 2005, pp. 255–262.

[23] K. Grove, "Critical point theory for distance functions," in *Differential geometry: Riemannian geometry (Los Angeles, CA, 1990)*, ser. Proc. Sympos. Pure Math. Amer. Math. Soc., Providence, RI, 1993, vol. 54, pp. 357–385.

[24] A. P. Morgan and A. J. Sommese, "Coefficient-parameter polynomial continuation," *Appl. Math. Comput.*, vol. 29, no. 2, part II, pp. 123–160, 1989.

[25] J. D. Hauenstein, A. J. Sommese, and C. W. Wampler, "Regeneration homotopies for solving systems of polynomials," *Math. Comp.*, vol. 80, no. 273, pp. 345–377, 2011.

[26] J. D. Hauenstein and J. I. Rodriguez, "Multiprojective witness sets and a trace test," *Adv. Geom.*, vol. 20, no. 3, pp. 297–318, 2020.

[27] P. E. Hart, N. J. Nilsson, and B. Raphael, "A formal basis for the heuristic determination of minimum cost paths," *IEEE transactions on Systems Science and Cybernetics*, vol. 4, no. 2, pp. 100–107, 1968.

[28] M. Plecnik, "Ellipse Synthesis of a Five-bar Linkage," in *ASME 2022 International Design Engineering Technical Conferences and Computers and Information in Engineering Conference*, St. Louis, Missouri, USA, 2022, pp. IDETC2022–91 341.